Multiwalled Carbon Nanotube Polymer Composites: Synthesis and Characterization of Thin Films

B. SAFADI,[1,2] R. ANDREWS,[1,2] E. A. GRULKE[1–3]

[1] Advanced Carbon Materials Center, University of Kentucky, Lexington, Kentucky

[2] Center for Applied Energy Research, University of Kentucky, Lexington, Kentucky 40511

[3] Chemical & Materials Engineering, University of Kentucky, Lexington, Kentucky 40506

Received 28 February 2001; accepted 15 August 2001

ABSTRACT: The aim of this article was to elucidate the basic relationships between processing conditions and the mechanical and electrical properties of multiwalled carbon nanotube reinforced polymer composites. In conventional chopped fiber reinforced polymer composites, uniform distributions of fibers throughout the matrix are critical to producing materials with superior physical properties. Previous methods have dispersed carbon nanotubes by aggressive chemical modification of the nanotubes or by the use of a surfactant prior to dispersion.[1,2] Here, ultrasonic energy was used to uniformly disperse multiwalled nanotubes (MWNTs) in solutions and to incorporate them into composites without chemical pretreatment. Polystyrene (PS) solutions containing MWNTs were cast and spun to yield thin film MWNT composites. The rheology of PS/MWNT suspensions was modeled using the Carreau equation. MWNTs were found to align at the shear rates generated by the spin casting process. The tensile modulus and strain to failure of samples compared well to classical micromechanical models, increasing with MWNT loading. The composite films showed lower strains at the yield stress than neat PS films. The presence of MWNTs at 2.5 vol % fraction approximately doubles the tensile modulus, and transforms the film from insulating to conductive (surface resistivity, ρ, approaching 10^3 $\Omega/\square$). © 2002 Wiley Periodicals, Inc. J Appl Polym Sci 84: 2660–2669, 2002

Key words: nanotubes; polymer-based nanocomposites; structural properties; shear alignment

INTRODUCTION

Since the discovery of carbon nanotubes by Iijima in 1991, tremendous effort has been expended to control their production and properties. Recent theoretical and experimental studies suggest that carbon nanotubes have remarkable mechanical and electrical properties.[3–7] These materials show great promise for many potential applications: for example, aerospace, nanoelectronics, and sporting goods. Our broad objectives are to explore the development of advanced composites in which carbon nanotubes serve as the reinforcing element in a polymer matrix. Although several studies have focused on producing polymer nanotube composites,[8–14] many practical challenges remain before their potential can be fully realized. Dispersing the nanotubes individually and uniformly into the matrix seems to be fundamental in producing composites with reproducible and optimal properties.

Correspondence to: R. Andrews (andrews@caer.uky.edu).

Journal of Applied Polymer Science, Vol. 84, 2660–2669 (2002)

Table I Properties of MWNTs and Other Carbon Fillers

Sample	Density (g/cm^3)	Diameter (d_{NT}) (nm)	Length (l_{NT}) (μm)	Aspect Ratio (l_{NT}/d_{NT})	Modulus E (GPa)	Reference
MWNTs	2.16	34	50	1471	450	[24]
General purpose carbon fibers P-400	1.5	10000	400	40	48	[25]
Graphite fibers F-600	1.5	9000	400	44	600	[25]
VGCFs (vapor grown carbon fibers)	1.8	200	3.6	18	240	[26]

In this article, we have investigated the effect of MWNT loading on mechanical and electrical properties of thin PS films without the use of sizing agents or other surface-active compounds. PS was chosen as the matrix material because its properties are well known; it is easy to process; it is soluble in a broad range of solvents; and its clarity allows dispersion of MWNTs to be observed at the micron scale. MWNTs were used as prepared[15] without any aggressive chemical pretreatment, purification, or modification, and dispersed using a simple sonication process. Thin composite films were formed by solvent casting or spin casting, and dried carefully prior to testing. Samples were characterized by scanning electron microscopy (SEM) to determine dispersion and orientation of MWNTs within the PS matrix. Composite samples were tested for tensile modulus (E_c) and yield strength. Surface resistivity (ρ_s), an important property for electronic shield and conducting applications, was also measured.

EXPERIMENTAL

The MWNTs used in this work were produced in a chemical vapor deposition reactor by the catalytic decomposition of hydrocarbons.[15] By control of the reaction conditions, the MWNTs can be produced in selectivities approaching 100%. Their mean external diameter, d_{NT}, is 30 nm, and their length, l_{NT}, ranges from 50 to 55 microns. Representory properties of as-produced MWNTs and other carbon reinforcements are summarized in Table I. Initially, MWNTs are dispersed in toluene using an ultrasonic wand dismembrator (Fisher Scientific 550) at 300 W for 30 min. The MWNT suspensions were then admixed with toluene solutions of 30% PS ($M_w \approx 280{,}000$, Scientific Polymer Products, Inc.), to yield 1 wt %, 2 wt %, and 5 wt % PS/MWNT solutions (final mixture concentrations of 15% PS in toluene). These mixtures were further homogenized in an ultrasonic bath for 30 min. (The duration was selected by determining the time needed to yield consistent viscosity measurements). The MWNT volume fraction, v_{NT}, was calculated to be 0.487 vol %, 0.98 vol %, and 2.49 vol % from the weight fractions 1 wt %, 2 wt %, and 5 wt %, respectively.

The viscosities of the nanotube dispersions were measured at room temperature using a Brookfield DVII+ viscometer over a range of shear rates and MWNT concentrations. Thin composite films were then produced from these solutions using two different techniques, film casting and spin casting.

Film Casting

Approximately 20 mL of each solution was poured into a flat-bottomed glass culture dish (100 mm in diameter by 10 mm in height), and the toluene allowed to evaporate. Thin uniform films with an average thickness of 0.4 mm were obtained and dried in a vacuum oven for 7 days at 80°C (below the PS glass transition temperature) and 25 in Hg vaccuum to completely remove any residual toluene. All films produced by this technique have a thickness greater than 150 microns, with most samples having an average film thickness of 400 μm.

Spin Casting

Spin casting is a three-step technique to produce uniform films: fluid is deposited at the center of the rotating disk; spinning accelerates the fluid and causes rapid thinning; and solvent evaporates from the film while the centrifugation continues. The PS/MWNT solutions were spun on a

Chemat Technology Spin Coater (KW-4A, 150 mm diameter) covered with Teflon-coated mold cloth. The Teflon-coated cloth was used to facilitate removal of the thin film from the disk once dried. Initially, 3 g of these suspensions were dispensed onto each substrate as a continuous stream at the center. Thin films of 30–50 μm in thickness were formed in 30 s at speeds ranging from 1000–2500 rpm. These films were subsequently dried for 7 days at 80°C in a vacuum oven at 25 in Hg vacuum. No bubbles were formed and fiber orientation remained unchanged during the drying process.

Structural Characterization

The MWNTs dispersion and orientation within the PS matrix were examined by scanning electron microscopy (SEM Hitachi 2700). The surface resistivity, ρ_s ($\Omega/\square$, ASTM D257-83), was measured using a surface resistance indicator (Prostat PSI 870). Strip samples were cut along chosen directions for both types of films as shown in Figure 1. Die cut dog bone test coupons (60 mm length and 3 mm width) were used for tensile testing. The composites investigated (at least 10 specimens per composition) were tested for tensile strength, elastic modulus, and strain to failure (according to ASTM D882-97) on a QT/1L Material Test System (MTS Corp.). The tensile machine was equipped with a 50 N full-scale load cell to assure linear response in the failure range of the tested specimens.

RESULTS AND DISCUSSION

The solvent casting technique gave thin films with random orientations of carbon nanotubes as observed by both optical microscopy and SEM evaluation. The cast films were uniform in thickness along their cross-section (averaging about 100–400 μm in thickness). MWNTs penetrated the surfaces of all films at all MWNT concentrations. The carbon nanotubes reflect light, and observation by optical microscopy show random orientations in the films (Fig. 2).

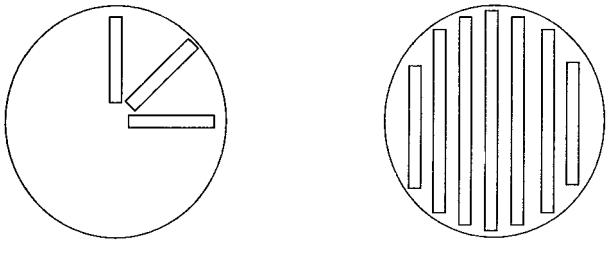

Figure 1 The selected configurations to prepare for tensile testing: (a) radial cut for spun films, and (b) chord cuts for cast films.

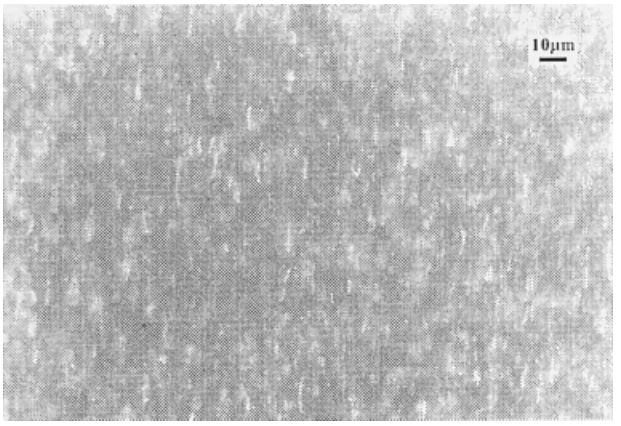

Figure 2 Optical microscope images of a PS/MWNT cast film.

The films produced by the spin casting technique had uniform thicknesses on the order of 50 μm (approximately the same as MWNT length). Fibers in polymer flows are known to be oriented by shear fields[16]; the velocity gradient of the spin casting system could cause nanotube orientation. The MWNT suspensions used in this work are shear thinning and thixotropic. The orientation results have been interpreted using rheological models for the suspension viscosity coupled with fluid flow models of the coating process, as discussed below.

Suspension Rheology and Spin Casting

Previous work on spin casting has considered Newtonian fluids,[17] power-law fluids,[18] Bingham plastics,[19,20] Carreau model fluids,[20] and micron-sized fiber suspensions.[21] Analysis of Newtonian[17] and Carreau[19] fluids without particulate inclusions showed that uniform films can be formed from non-uniform initial profiles, and that the final film thickness is independent of the initial profile, but does depend on spinning time. By contrast, Acrivos et al.[18] showed theoretically that power-law fluids could not form uniform films, which was extended by Jenekhe and Shuldt.[20] The power law model predicts infinite viscosities at the limit of zero shear rates, so that finite centrifugal forces cannot deform the fluid.

The Carreau model, in contrast, has a limiting Newtonian viscosity at low shear rates. Our results, in which uniform films were formed despite non-uniform initial profiles, suggest that a Carreau model would be preferred for describing the effects of shear rate on suspension viscosity.

Franke and Birnie[21] reported the orientation of micron-sized Al_2O_3 fibers (10 μm diameter, aspect ratio of 50) suspended in a transparent oil (presumably a Newtonian fluid) with a viscosity of 47.5 cP under the spin casting conditions. Using optical microscopy, the authors found that the fibers were highly oriented in the radial direction near the center of the disk, while they became oriented perpendicular to the radial direction near the outside diameter of the disk.[21] High numbers of fibers existed near the disk center, while fewer existed near the outer diameter, presumably due to ejection from the spinning disk. The fiber orientation was attributed to two effects: the velocity gradient through the film thickness, $\partial v_r/\partial z$, and the radial velocity gradient at constant film height due to the different position of the fiber ends. The vertical velocity gradients would tend to align the fibers in the radial direction, while the radial velocity gradient would tend to align fibers perpendicular to the radial direction. When the film height is less than that of the fiber length, the fiber would lie flat on the surface and might align perpendicular to the radial direction, as fluid would force it toward the edge of the disk. These two mechanisms may have dominated in the Franke and Birnie work,[21] since the minimum fiber dimension (10 μm) was much greater than the expected film thickness for a Newtonian fluid in radial flow (0.1 μm, from Emslie et al.[17])

By contrast, the MWNTs had diameters that were much less than the film thickness: $d_{NT} \ll L_{NT}$. However, the fiber length and the film thickness were the same order of magnitude: $h \approx L_{NT}$. These differences in the relationship between fiber and film dimensions seem likely to result in different flow mechanisms affecting fiber orientation.

Flow Analysis

Velocity gradients give rise to shear within the film, which can orient the MWNTs. The shear stress and viscosity model can be used to determine the velocity gradient as a function of film height and radial distance. Following previous analyses, assumptions describing the film forming process are:

1. The flow is incompressible and non-Newtonian:
$$\tau_{rz} = -\eta\dot{\gamma} \tag{1}$$
τ_{rz} is the radial component of shear stress and $\dot{\gamma}$ the shear rate.[20]
2. Gravitational effects are negligible in the liquid flow compared to the centrifugal forces.[20]
3. The system can be considered as 2π periodic and all variables reduced to functions of disk radius, r[17].

Emslie et al.[17] modeled the spin casting process with the basic equations:

$$\frac{\partial \tau_{rz}}{\partial z} = \rho\omega^2 r \tag{2}$$

$$\dot{\gamma} = \frac{\partial v_r}{\partial z} \tag{3}$$

$$\tau_{rz} = -\eta \frac{\partial v_r}{\partial z} \tag{4}$$

where v_r is the radial velocity, ρ the fluid density, ω the rotational speed of the disk, r the radial position within the spinning disk, and z the height within the film which ranges from 0 at the substrate to h, the final film thickness. This solution was extended by Jenekhe and Shuldt[20] for a Carreau fluid, yielding:

$$\eta = -\eta_0\left[1 + \lambda^2\left(\frac{\partial v_r}{\partial z}\right)^2\right]^{(n-1)/2}, \quad n < 1 \tag{5}$$

where η_0 is the zero shear rate viscosity, n the Newtonian index, and λ the time constant of a Carreau fluid. The shear stress is consequently found to be:

$$\tau_{rz} = -\eta_0[1 + \lambda^2\dot{\gamma}^2]^{(n-1)/2}\dot{\gamma} \tag{6}$$

Governing boundary conditions at the disk surface is:

$$z = 0, \quad v_r = 0, \tag{7a}$$

and at the free surface:

$$z = h, \ \tau_{rz} = 0. \tag{7b}$$

Combining eqs. (2),(4), (7a) and (7b) gives

$$\tau_{rz} = \rho\omega^2 r(h - z) \tag{8}$$

which describes the shear stress in the flow field, and can be used in conjunction with the viscosity model to define the shear rate and the local velocity profile. The velocity distribution that satisfies eqs. (4) and (8), and the boundary conditions (7a) and (7b) is:

$$v_r = \int_0^z \frac{\rho\omega^2 r}{\eta}\,(h - z')\,dz' \tag{9}$$

which integrates for a constant viscosity as

$$v_r = \frac{\rho\omega^2 r}{\eta}\left(hz - \frac{z^2}{2}\right) \tag{10}$$

Effects of Coriolis Forces

Most analyses of the shearing forces in spin casting (see for example Emslie et al.[17]) assume that the Coriolis acceleration,

$$a_{\text{cor}} = 2\omega v_r, \tag{11}$$

of the fluid is small compared to the viscous acceleration,

$$a_{\text{vis}} = \omega^2 r. \tag{12}$$

This condition is then

$$2\omega v_r \ll \omega^2 r. \tag{13}$$

According to eq. (10), a maximum radial velocity at a given radius, r, occurs when $z = h$. Therefore,

$$v_{r\max} = \frac{\rho\omega^2 r h^2}{2\eta}, \tag{14}$$

and the Coriolis limits becomes

$$\eta \ll \rho\omega h^2. \tag{15}$$

Carreau Model for PS/MWNT Suspensions

Figure 3 shows experimental data and Carreau model fit for PS/MWNT solutions. The fits were obtained by nonlinear regression and the resulting coefficients are given in Table II. The neat polystyrene solution is Newtonian ($n \sim 1$). The PS/MWNT suspensions are shear thinning and have $n < 1$. As the nanotube loading increases, n decreases and the product, $\eta_0\lambda^{n-1}$, equivalent to the consistency index in the power-law model, is increasing.

Table II Carreau Model Parameters

Sample	λ (s)	η_0 (Pa · s)	n
Blank PS	4546	2.223	0.986
PS + 1% wt. MWNTs	7.5	11.19	0.718
PS + 2% wt. MWNTs	2651.7	4076	0.393
PS + 5% wt. MWNTs	15150	43200	0.356

MWNT Orientation

Alignment of the MWNTs caused by the spin casting process was also characterized. Thin films containing 5 wt % of MWNTs were spun at speeds of 1000 and 2200 rpm. SEM images of samples cut perpendicular to a radial position within the films, and grouped into two ranges of distance from the rotation axis (0–5 mm and 35–50 mm) were analyzed. For each image, the orientation angle of each visible nanotube was measured with respect to an arbitrary zero direction. The relative frequency of orientation angles was found to have a bimodal distribution in all cases. A Gaussian function (Fig. 4) was applied to fit the distribution of the relative frequency as a function of the orientation angle. An orientation angle of 0° means that the nanotube is aligned parallel to the disk radius.

Table III shows that the MWNTs were aligned in specific angles relative to the radial direction: 45°, and 135°, on average. The orientation averages were within three standard errors of these angles. Alignment took place at all rotational velocities and locations on the disk. In each case, the assumption of the condition for neglecting Coriolis effects (eq. 17) was met, that is, the viscosity was orders of magnitude greater than the Coriolis limit. Shear alignment must occur at shear stress less than 0.8 Pa, but no lower rotating speeds were tested. As mentioned previously, the disk surface of these films showed no preferential alignment and had random orientation of the fibers. Because of their high aspect ratio, MWNTs can interact physically at very low volume fractions in suspension (about 0.000018 based on a

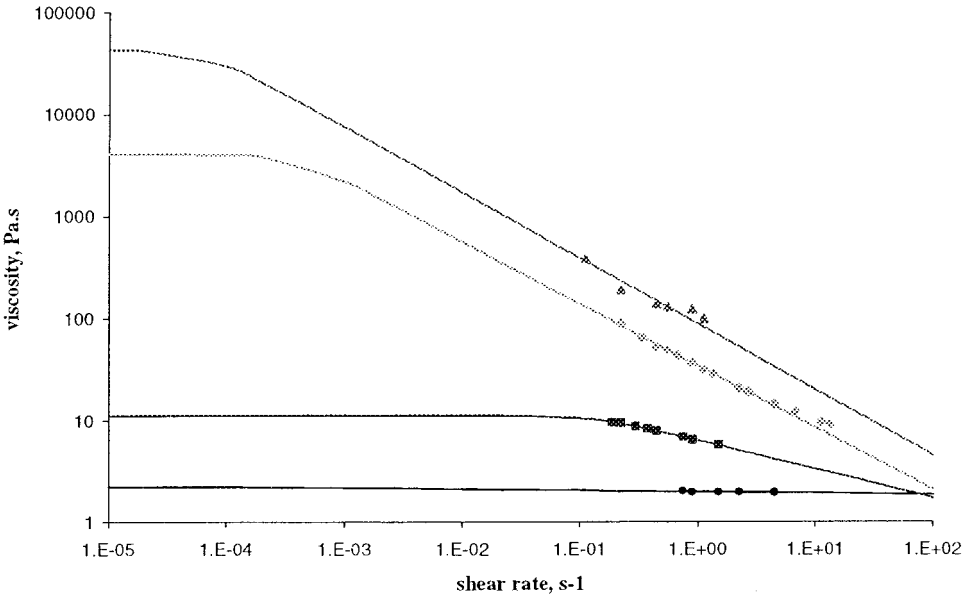

Figure 3 The suspension viscosity as a function of shear rate. Calculated (lines) and experimental values (symbols) for PS/MWNT solutions at different nanotube concentrations: (♦) 5 % wt., (■) 2 % wt., (▲) 1 % wt., and (●) neat PS solution. Carreau model parameters are given in Table II.

radius of gyration calculation for these particular samples). Since most practical systems will be at volume fractions much greater than this volume fraction, fiber–fiber interactions are expected during flow orientation.

Electrical Properties

Figure 5 shows the decrease in surface resistivity with MWNTs volume fraction (v_{NT}) for cast and spun films. While blank PS films are insulating

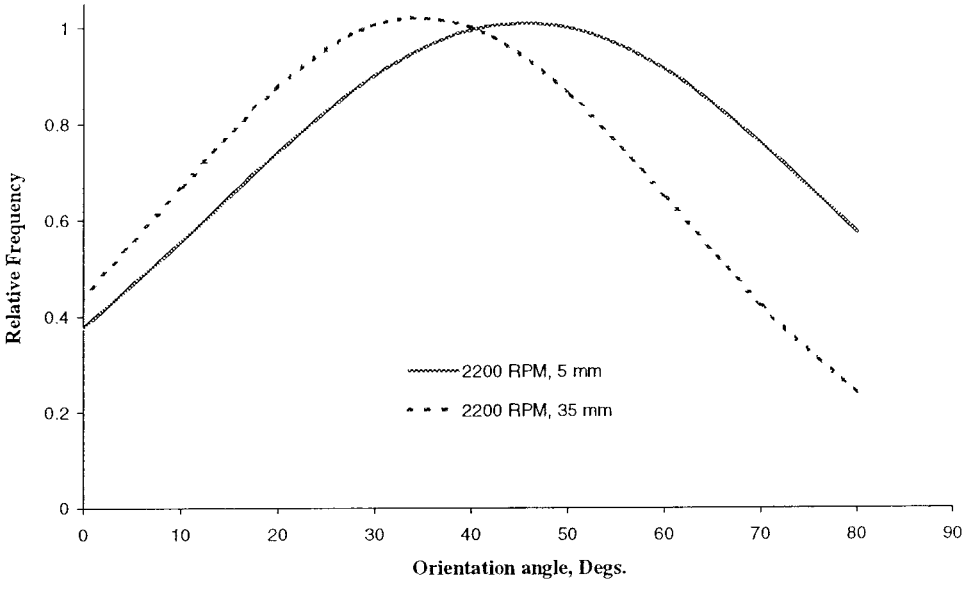

Figure 4 Relative alignment of nanotubes to rotation disk radius within a thin composite film doped with 5 wt. %and spun at 2200 rpm.

Table III Shear Alignment Data

Spinning Speed (rpm)	Radial Position (mm)	Shear Stress (Pa)	Coriolis Limits $\rho\omega h^2$	Average Orientation Angle (°)
1000	5	0.81	9.57E-05	44 ± 1.94 142.1 ± 1.77
1000	35	5.66	2.11E-04	52.9 ± 5.89 136.7 ± 4.39
2200	5	3.91	9.57E-05	44.5 ± 3.68 140.6 ± 1.75
2200	35	27.38	2.11E-04	55.4 ± 4.65 145.7 ± 4.99

materials[22] ($\geq 10^{12}$ Ω/ □), increasing the MWNT content transformed them to highly conductive compounds (approaching 10^3 Ω/□ at 2.49 vol % of MWNTs). The intrinsic properties of the MWNTs lower the volume fraction necessary to reach the percolation threshold compared to traditional carbon black fillers or graphite fibers. Besides their highly conductive graphitic structure, MWNTs have a higher aspect ratio (~ 1500 in this case), establishing an efficient conducting network inside the matrix at much lower concentrations. The alignment of the spun films did not alter the electrical properties relative to those of the cast films. This likely results from the three-dimensional network of nanotubes that exists at these loadings in both types of fibers. The composites may find applications as anti-static materials, in electrostatic painting, or as protective coatings for electronic components.

Mechanical Characterization

Table IV and Table V present the tensile strength and elastic modulus measured experimentally as a function of MWNT concentration. The mechanical properties of spun and cast films were essentially the same, suggesting that the three-dimensional distribution of nanotubes controlled the failure mechanism. The tensile analysis leads to the following observations:

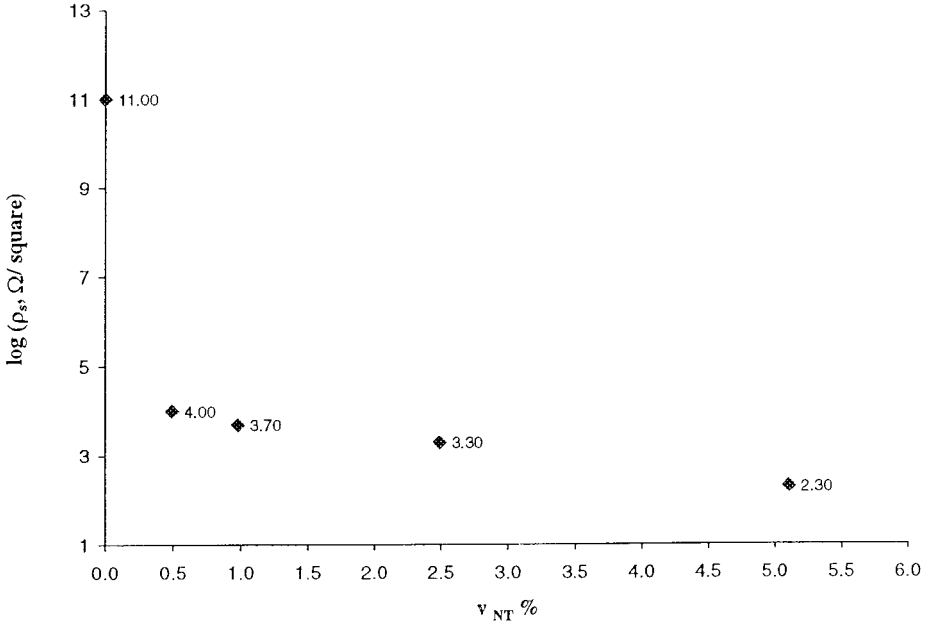

Figure 5 Surface resistivity, ρ_s, plotted as a function of MWNT volume fraction v_{NT}.

Table IV Properties of Cast Nanotube Composite Films

Sample	Volume Fraction of Filler (vol %)	Elastic Modulus (MPa)	Tensile Strength (MPa)
Blank PS	—	1530 ± 110	19.5 ± 3.0
PS + 1% wt. MWNTs	0.487	2100 ± 180	24.5 ± 3
PS + 2% wt. MWNTs	0.98	2730 ± 220	25.7 ± 1.2
PS + 5% wt. MWNTs	2.49	3400 ± 190	30.6 ± 2.7

1. Modulus increases with increasing MWNT concentration. Compared to neat PS films, an addition of 2.49 vol % of MWNTs improves the moduli by factors of 2 for cast and spun films.
2. Tensile strength increases with carbon nanotube concentration.

PS / MWNT composite films can be considered, as a first approximation, as randomly oriented discontinuous fiber lamina.[14] The elastic modulus, E_c, of the composite can be calculated according to the following equations[23]:

$$E_c = \left[3/8 \, \frac{1 + 2(1_{NT}/d_{NT})\eta_L v_{NT}}{1 - \eta_L v_{NT}} + 5/8 \, \frac{1 + 2\eta_T v_{NT}}{1 - \eta_T v_{NT}} \right] E_{PS} \quad (16)$$

$$\eta_L = \frac{(E_{NT}/E_{PS}) - 1}{(E_{NT}/E_{PS}) + 2(l_{NT}/d_{NT})} \quad (17)$$

$$\eta_T = \frac{(E_{NT}/E_{PS}) - 1}{(E_{NT}/E_{PS}) + 2} \quad (18)$$

E_{PS} and E_{NT} (Table I) represent tensile modulus of blank PS and MWNTs, v_{NT} the volume fraction of MWNTs, l_{NT} their length and d_{NT} their diameter.

Experimental values for the modulus are in close agreement with the theoretical calculations (Fig. 6). However, at higher nanotube volume fractions (more than 2.5 vol %) the deviation from the model is greater. The reason for this difference is being studied further. SEM images (Fig. 7) of the fractured surface of tested samples show that some MWNTs have fractured and some have pulled out perpendicular to the matrix. Some plastic deformation of the fracture surface is also visible. Failure of the nanotube–matrix interface (pull-out) may be associated with the stiffness of nanotubes. At less than 1 vol % of MWNTs, the derived composites present an increase of approximately 40% in tensile strength above the neat polymer, realizing the reinforcement effect expected from the nanotubes.

In conclusion, there are two possible failure modes: breakage or pull-out. For poor nanotube–matrix bonding, under applied loads, MWNTs can act as defects within the material and consequently be sites for cracking and subsequent fracture. If the adhesion between the matrix and the nanotubes is strong, the external loads are then transferred to the nanotubes, resulting in high performance polymer–nanotube composites.

CONCLUSIONS

Thin films of MWNT-filled composites (0.5–2.5 vol. %) can be fabricated and oriented using spin

Table V Properties of Spun Nanotube Composite Films

Sample	Volume Fraction of Filler (vol %)	Elastic Modulus (MPa)	Tensile Strength (MPa)
Blank PS	—	1530 ± 110	19.5 ± 3.0
PS + 1% wt. MWNTs	0.487	2060 ± 230	18.6 ± 2
PS + 2% wt. MWNTs	0.98	2720 ± 170	23.2 ± 1.9
PS + 5% wt. MWNTs	2.49	3370 ± 190	26.0 ± 2.6

casting methods. Uniform dispersions of MWNTs are required for reproducible fluid flow and orientation. Such dispersions can be accomplished using a simple sonication process. MWNT orientation is higher near the high shear surface (fluid–solid interface), and decreases to random orientation at the shear-free fluid–air interface.

Composites with up to one volume percent MWNT loading have the expected increase in tensile strength. However, there were no statistically differences between the composite mechanical properties based on the orientation of the MWNTs. All composite samples exhibited metallic conductivity, suggesting that the percolation threshold is less than 0.5 vol. %.

This work was funded by the National Science Foundation, Division of Materials Research under grant no. DMR-9809686.

NOMENCLATURE

d_{NT}	nanotube diameter (nm)
E_c	elastic modulus of a PS / MWNT composite
E_{NT}	elastic modulus of one MWNT
E_{PS}	elastic modulus of a neat PS film
h	film thickness (m)
l_{NT}	nanotube length (μm)
n	Newtonian index
r	radial position (m)
v_{NT}	nanotube volume fraction
v_r	radial component of velocity (m/s)
z	film height (m)

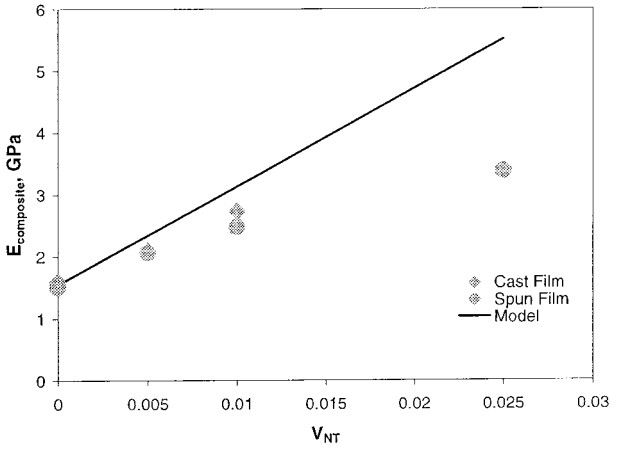

Figure 6 Comparative plot of composite elastic modulus, E_c, as a function of nonotube volume content, v_{NT}, for cast and spun PS/MWNT films.

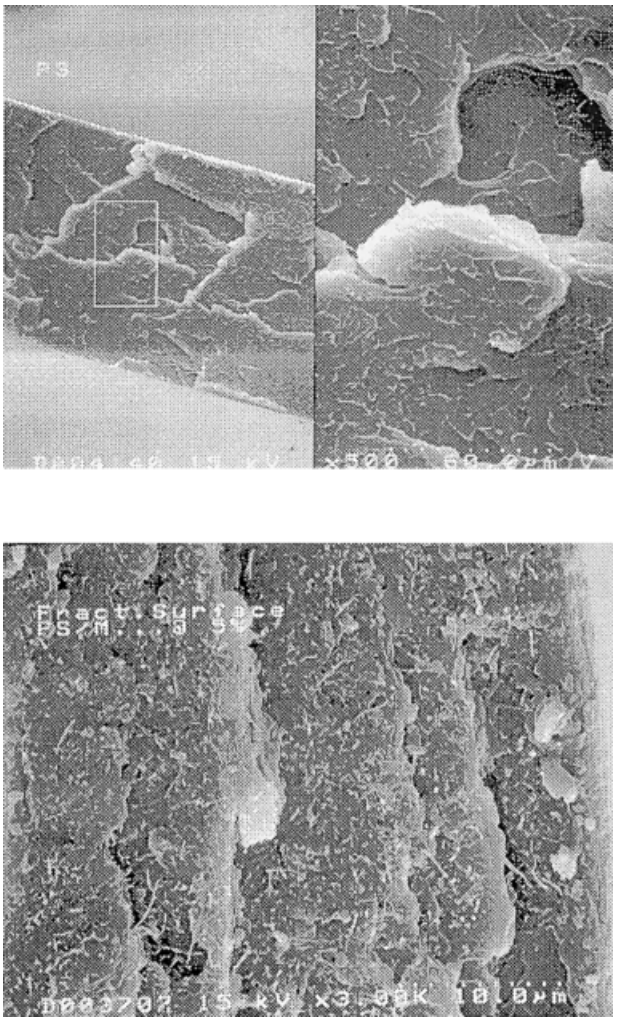

Figure 7 SEM images of fractured surfaces in tested specimens: (a) neat PS, and (b) PS with 5 wt % if MWNTs showing individually dispersed nanotubes.

Greek Letters

$\dot{\gamma}$	shear rate (s^{-1})
η	fluid viscosity (Pa · s)
η_0	zero-shear viscosity (Pa · s)
λ	time constant of a Carreau fluid (s)
ρ_s	surface resistivity ($\Omega/\square$)
ρ	density (kg/m^3)
τ_{rz}	radial component of the shear stress (Pa)
ω	angular velocity of spinning disk (rad/s)

REFERENCES

1. Shaffer, M. S. P.; Fan, X.; Windle, A. H. Carbon 1998, 36, 1603.
2. Gong, X.; Liu, J.; Baskaran, S.; Voise, R. D.; Young, J. S. Chem Mater 2000, 12, 1049.

3. R. S. Ruoff, D. C. Lorents Carbon 1995, 33, 925.
4. Mintmire, J. W.; White, C. T. Carbon 1995, 33, 893.
5. Treacy, M. M. J.; Ebbesen, T. W.; Gibson, J. M. Nature 1996, 381, 678.
6. Wong, E. W.; Sheehan, P. E.; Lieber, C. M. Science 1997, 277, 1971.
7. Poncharal, P.; Wang, Z. L.; Ugarte, D.; de Heer, W. A. Science 1999, 283, 1513.
8. Ajayan, P. M.; Stephan,O.; Colliex, C.; Trauth, D. Science 1994, 265, 1212.
9. Wagner, H. D.; Lourie, O.; Feldman, Y.; Tenne, R. Appl Phys Lett 1998, 72, 188.
10. Jin, L.; Bower, C.; Zhou, O. Appl Phys Lett 1998, 73, 1197.
11. Schadler, L. S.; Giannaris, S. C.; Ajayan, P. M. Appl Phys Lett 1998, 73, 3842.
12. Sandler, J.; Shaffer, M. S. P.; Prasse, T.; Bauhofer, W.; Schulte, K.; Windle, A. H. Polymer 1999, 40, 5967.
13. Bower, C.; Rosen, R.; Jin, L.; Han, J.; Zhou, O. Appl Phys Lett 1999, 74, 3317.
14. Qian, D.; Dickey, E. C.; Andrews, R.; Rantell, T. Appl Phys Lett 2000, 76, 2868.
15. Andrews, R. Jacques, D.; Rao, A. M.; Derbyshire, F.; Qian, D.; Fan, X.; Dickey, E. C. Chen, J. Chem Phys Lett 1999, 303, 467.
16. Khan S. A.; Prud'homme, R. K. Rev Chem Eng 1987, 4, 205.
17. Emslie, A. G.; Bonner, F. T.; Peck, L. G. J Appl Phys 1958, 29, 858.
18. Acrivos, A.; Shah, M. J.; Petersen, E. E. J Appl Phys 1960, 31, 963.
19. Matsumoto, S.; Takashima, Y.; Kamiya, T.; Kayano A.; Ohta, Y. Ind Eng Chem Fundam 1982, 21, 198.
20. Jenekhe, S. A.; Schuldt, S. B. Ind Eng Chem Fundam 1984, 23, 432.
21. Franke, E. K.; Birnie III, D. P. J Mat Sci Lett 1995, 14, 1807.
22. Scobbo, J. J.; Proceedings of ANTEC'98; Society of Plastics Engineers: Atlanta, GA, 1998; p 2468.
23. Mallick, P. K. Fiber-Reinforced Composites, 2nd ed.; Marcel Dekker: New York, 1993, p 130.
24. Pan, Z. W.; Xie, S. S.; Lu, L.; Chang, B. H.; Sun, L. F.; Zhou, W. Y.; Wang, G.; Zhang, D. L. Appl Phys Lett 1999, 74, 3152.
25. Chung, D. L. Carbon Fiber Composites; Butterworth-Heinmann: Boston, MA, 1994, p 8.
26. Tibbetts, G. G.; Mchugh, J. J. J Mater Res 1999, 14, 2871.